Journal of Thermal Analysis and Calorimetry (2019) 137:965–982
https://doi.org/10.1007/s10973-019-08012-2

Mixed convection flow caused by an oscillating cylinder in a square cavity filled with Cu–Al_2O_3/water hybrid nanofluid

S. A. M. Mehryan[1] · E. Izadpanahi[2] · M. Ghalambaz[3] · A. J. Chamkha[4,5]

Received: 3 September 2018 / Accepted: 7 January 2019 / Published online: 25 January 2019

Abstract

The aim of this paper is to examine the effects of Cu–Al_2O_3/water hybrid nanofluid and Al_2O_3/water nanofluid on the mixed convection inside a square cavity caused by a hot oscillating cylinder. The governing equations are first transformed into dimensionless form and then discretized over a non-uniform unstructured moving grid with triangular elements. The effects of several parameters, such as the nanoparticle volume fraction, the Rayleigh number, the amplitude of the oscillation, and the period of the oscillation of the cylinder are investigated numerically. The results indicate that the motion of the oscillating cylinder toward the top and bottom walls increases the average Nusselt number when the Rayleigh number is low. Furthermore, the presence of Al_2O_3 and Cu–Al_2O_3 nanoparticles leads to an increase in the values of the average Nusselt number Nu_{avg} for cases of low values of the Rayleigh number. It is found that the natural convection heat transfer rate of a simple Al_2O_3/water nanofluid is better than that of Cu–Al_2O_3/water hybrid nanofluid.

Keywords Hybrid nanofluid · Oscillatory cylinder · Nanofluid · Nanoparticles · Mixed convection

List of symbols

A	Amplitude of oscillation
C_p	Specific heat at constant pressure
D	Diameter of the cylinder
f	Dimensionless frequency ($f = \omega L^2/\alpha_f$)
g	Gravity acceleration
k	Thermal conductivity
L	Length of the cavity
Nu	Nusselt number
P	Pressure
Pr	Prandtl number ($Pr = \nu/\alpha$)
R	Radius of the cylinder
Ra	Rayleigh number ($Ra = g\beta(T_H^* - T_C^*)L^3/\nu\alpha$)
T	Temperature
T_P	Period of oscillation ($T_P = 1/f$)
t	Dimensional time
x, y	Cartesian coordinates
u	Velocity component along x-axis
v	Velocity component along y-axis
$\mathbf{w}$	Velocity of the moving grid
W_0	The length of the cylindrical heater

✉ M. Ghalambaz
m.ghalambaz@gmail.com; m.ghalambaz@iaud.ac.ir

S. A. M. Mehryan
alal171366244@gmail.com

E. Izadpanahi
eizad001@fiu.edu

A. J. Chamkha
achamkha@pmu.edu.sa

[1] Young Researchers and Elite Club, Yasooj Branch, Islamic Azad University, Yasooj, Iran

[2] Department of Mechanical and Materials Engineering, Florida International University, Miami, FL 33174, USA

[3] Department of Mechanical Engineering, Dezful Branch, Islamic Azad University, Dezful, Iran

[4] Mechanical Engineering Department, Prince Mohammad Endowment for Nanoscience and Technology, Prince Mohammad Bin Fahd University, Al-Khobar 31952, Saudi Arabia

[5] RAK Research and Innovation Center, American University of Ras Al Khaimah, P.O. Box 10021, Ras Al Khaimah, United Arab Emirates

Greek symbols

α Thermal diffusivity
β Thermal expansion coefficient
μ Dynamic viscosity
ν Kinematic viscosity
ρ Density
τ Dimensionless time ($\tau = t\alpha_f/L^2$)
φ Volume fraction
ω Dimensional frequency

Superscripts

* Dimensional parameters

Subscripts

avg Average
C Cold
H Hot
f Base fluid
nf Nanofluid
hnf Hybrid nanofluid
hnp Hybrid nanoparticles

Introduction

Natural convection induced by a circular cylinder inside a square cavity has been thoroughly investigated due to its variety of applications in engineering systems, such as in the cooling of electronic devices, in heat exchangers, in solar collectors, in chemical reactors, and in refrigerator condensers. Cesini et al. [1] reported both numerical and experimental results of natural convection caused by a horizontal cylinder in a rectangular cavity. Natural convection caused by two hot inner circular cylinders inside an enclosure has been investigated by Yoon et al. [2]. They found that the transition from steady-state natural convection to an unsteady state depends on the Rayleigh number and the location of the cylinder inside the enclosure. The same conclusion was also reported by Kim et al. [3], Park et al. [4], Kang et al. [5] and Doo et al. [6], indicating that the bifurcation from steady state to unsteady state and vice versa depends on the location of the cylinder inside the enclosure. Huang et al. [7] reported the effects of the time-periodic pulsating temperature of a cylinder on the natural convection inside a square cavity. They found that heat transfer was enhanced compared to steady-state natural convection. The effect of an elliptic cylinder on the natural convection inside an inclined square enclosure was investigated numerically by Zhang et al. [8] using the Galerkin finite element method. They reported that the Rayleigh number, the size of the inner cylinder and the inclination angle of the outer square enclosure have a significant impact on the streamlines and the temperature contours. Comprehensive investigations have been performed regarding the effects of the inner cylinder on the heat transfer and fluid flow inside an enclosure [9–12].

Since nanofluids were introduced by Choi [13], a great many studies have been done regarding the effects of nanofluids on heat transfer and fluid flow. Nanofluids are now widely utilized in different thermal systems to enhance the heat transfer characteristics of those systems. Nanofluids are produced by the dispersion of nanometer-sized particles in a base fluid. The most common base fluids are usually conductive fluids such as water, oils, ethylene glycol, bio-fluids, polymer solutions, and other lubricants. The nanoparticles can mostly be classified into two categories, comprising metallic particles (Cu, Al, Fe, Au, and Ag) and non-metallic particles (Al_2O_3, CuO, Fe_3O_4, TiO_2, and SiC). Non-metallic particles, such as Al_2O_3, have better stability and chemical inertness; however, they have lower thermal conductivity compared to metallic nanoparticles. Kahveci [14] studied five types of nanoparticles inside a differentially heated, tilted enclosure. He reported that the average heat transfer rate of metallic nanoparticles was higher than that of non-metallic nanoparticles. In contrast, metallic nanoparticles have much higher thermal conductivities, but they suffer from poor stability and a high tendency to chemical reactions.

Different aspects of the convective heat transfer of nanofluids have been reported by different authors. The convective heat transfer of nanofluids in a cavity has been addressed by Garoosi et al. [15, 16]. The boundary layer heat transfer of nanofluids has been studied in [17], and the MHD heat transfer of nanofluids has been investigated in [18–22]. Mahian et al. [23, 24] reviewed the heat transfer mechanisms of nanofluids. The convective heat transfer of nanofluids has been also studied in microchannels [25] and between parallel plates [26].

The effect of a nanofluid on natural convection inside a cavity has been reported by several authors [27–35]. Abu-Nada et al. [29] and Bondareva et al. [34] have considered mixed convective effects in a cavity. Sheremet et al. [31] reported on the effect of the presence of porous media in the cavity. Mansour et al. [33], Sheremet et al. [35], Rashad et al. [36] and Alsabery et al. [37] investigated the effect of the presence of nanoparticles on the MHD convective heat transfer of nanofluids in a cavity. Ismael and Ghalib [38] studied the double-diffusive effects of heat and mass transfer in a cavity. Alsabery and coworkers investigated the unsteady effects [39] and the effect of the presence of a rotating cylinder [40, 41] on the heat transfer of a cavity. The conjugate heat transfer of nanofluids has been addressed by Sheremet et al. [30] and Alsabery et al. [42]. Heat transfer of nanofluids in conjugate heat transfer applications has also been studied in the literature [43, 44].

As we see, many aspects of the heat transfer of nanofluids have already been addressed in the literature. However, hybrid nanofluids are a new type of nanofluids that incorporate a small amount of metal nanoparticles alongside non-metallic nanoparticles. Hybrid nanofluids outstandingly show enhanced thermal properties. Jeena et al. [45] prepared a copper–alumina composite briquette from a homogeneous mixture of finely divided CuO and Al_2O_3 using a hydrogen reduction technique. Suresh et al. [46] reported a significant augmentation in viscosity and also found that the change in viscosity was higher than the increase in thermal conductivity. There are some studies that have investigated natural convection phase change heat transfer of hybrid nanofluids such as [47–49]. Suresh et al. [50] obtained a maximum enhancement of 13.56% in the Nusselt number for a Cu–Al_2O_3 hybrid nanofluid. Ismael et al. [51] have investigated the mixed convection and entropy generation of hybrid nanofluids in a lid-driven cavity. Hemmat et al. [52] used Ag–MgO/water hybrid nanofluid with a nanoparticle volume fraction range between 0% and 2%. They compared the thermal conductivity and the dynamic viscosity obtained by theoretical and empirical correlations with experimental data. The effects of water-based Al_2O_3 and Cu–Al_2O_3 hybrid nanofluid with 0.1% volume concentration on laminar forced convective heat transfer was investigated by Moghadassi et al. [53]. Their results indicated that the hybrid nanofluid has a much larger convective heat transfer coefficient. Mehryan et al. [54] investigated the natural convection of hybrid nanofluids in porous media.

Due to the significant applications of a square cavity with an inner hot cylinder in thermal and engineering systems, there is great interest in learning how to enhance its thermal performance. Accordingly, in this paper, the effects of Cu–Al_2O_3/water hybrid nanofluid and Al_2O_3/water nanofluid, as well as other parameters including the Rayleigh number, the amplitude of the cylinder oscillation, and the period of the oscillation of the cylinder on the natural convection inside an enclosure with a hot inner cylinder are studied. The present study aims to address the effect of the presence of nanoparticles and their volume fraction on the heat transfer rate and the heat and flow patterns in a cavity. Moreover, the effect of the cylinder oscillation (period and amplitude) on the heat transfer rate (time-averaged Nusselt number) for a pure fluid, a nanofluid and a hybrid nanofluid will be analyzed.

The mathematical model

The schematic diagram of the problem under investigation is displayed in Fig. 1. The square cavity enclosure shown (length = width = L) consists of an oscillation cylinder (with diameter D = 2R = 0.2L) with the high temperature of T_H*. All the external walls of the cavity are held at the cold temperature of T_C*. The cavity is filled with a Cu–Al_2O_3/water hybrid nanofluid and an Al_2O_3/water nanofluid. All kinds of nanofluids are supposed to be Newtonian, incompressible and viscous. The fluid flow is in the range of the laminar flow. Here, it is also assumed that the base fluid and the nanoparticles are in both thermal and dynamic equilibria. The nanoparticles are always suspended and stable, which means that there is no agglomeration or sedimentation. With the exception of the density of the nanofluid in the buoyancy term in the momentum equation, all the thermophysical properties of the base fluid and the nanoparticles of Cu and Al_2O_3 (shown in Table 1) are constant. The Boussinesq approximation is utilized to simulate the variations of density in the buoyancy term. The gravity acceleration is applied in the negative y-direction. The viscous dissipation and radiation effects are neglected in comparison with the convection and conduction terms in the energy equation. The swinging cylinder oscillates in the y-direction, so that its prescribed displacement is defined as $y = A^* \sin 2\pi\omega t$, in which A^* and ω are the amplitude and the ordinary frequency, respectively.

Considering the above assumptions, the governing equations can be represented as follows:

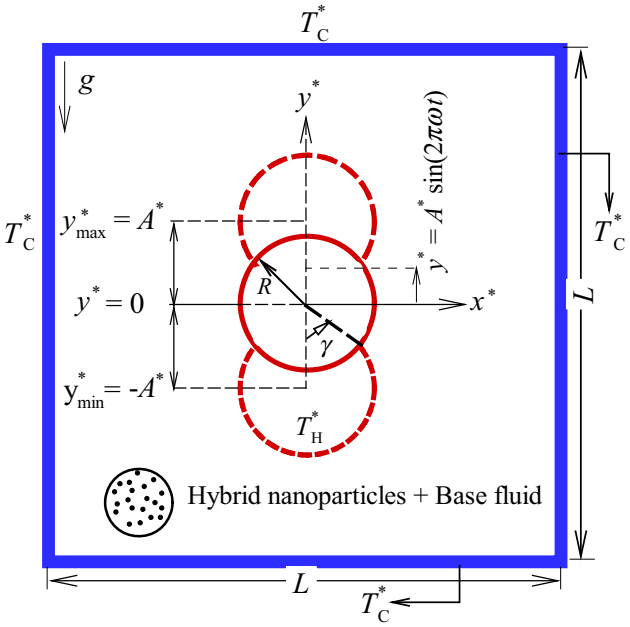

Fig. 1 The schematic diagram of the present problem

Continuity equation

$$\nabla^* \cdot \mathbf{u}^* = 0 \tag{1}$$

Momentum equation

$$\frac{\partial \mathbf{u}^*}{\partial t} + (\mathbf{u}^* - \mathbf{w}^*) \cdot \nabla^* \mathbf{u}^* = -\frac{1}{\rho_{\text{hnf}}} \nabla^* P^* + \frac{\mu_{\text{hnf}}}{\rho_{\text{hnf}}} \nabla^{*2} \mathbf{u}^* + \beta_{\text{hnf}} \mathbf{g}\left(T^* - T_{\text{C}}^*\right) \tag{2}$$

Energy equation

$$\frac{\partial T^*}{\partial t} + (\mathbf{u}^* - \mathbf{w}^*).\nabla^* T^* = \alpha_{\text{hnf}} \nabla^{*2} T^* \tag{3}$$

In the above-mentioned equations, u^* is the velocity vector with the components of u and v in x- and y-directions, respectively. w^* is the velocity of the moving grid, P^* is the fluid pressure, T^* is the fluid temperature, and g is the gravity acceleration vector. α_{hnf} and μ_{hnf} are the thermal diffusivity and the dynamic viscosity of the hybrid nanofluid, respectively. ρ_{hnf} is the density of the hybrid nanofluid, and β_{hnf} is the volumetric thermal expansion coefficient of the hybrid nanofluid. The boundary and initial conditions imposed on the domain are:

On all the external walls of the cavity $T^* = T_{\text{C}}^*$ and $u^* = v^* = 0$ (4)

On the oscillating cylinder $T^* = T_{\text{H}}^*$ (4b)

On the oscillating cylinder $u^* = 0$ and $v^* = \dfrac{\mathrm{d}y^*}{\mathrm{d}t} = 2A^*\pi\omega\cos(2\pi\omega t)$ (4c)

The steady-state solution for a fixed cylinder at the center of the cavity is considered as the initial condition.

Using the following non-dimensional parameters:

$$\tau = \frac{t\alpha_{\text{f}}}{L^2}, \quad x = \frac{x^*}{L}, \quad x = \frac{y^*}{L}, \quad \mathbf{u} = \frac{\mathbf{u}^* L}{\alpha_{\text{f}}}, \quad \mathbf{w} = \frac{\mathbf{w}^* L}{\alpha_{\text{f}}},$$
$$P = \frac{L^2}{\rho_{\text{f}}\alpha_{\text{f}}^2} P^*, T = \frac{T^* - T_{\text{C}}^*}{T_{\text{H}}^* - T_{\text{C}}^*}, \quad \nabla = \frac{\nabla^*}{1/L}, \quad \nabla^2 = \frac{\nabla^{*2}}{1/L^2},$$
$$Pr = \frac{\nu_{\text{f}}}{\alpha_{\text{f}}}, \quad Ra = \frac{g\beta(T^* - T_{\text{C}}^*)L^3}{\nu_{\text{f}}\alpha_{\text{f}}} \tag{5}$$

yields the following non-dimensional equations:

$$\nabla \cdot \mathbf{u} = 0 \tag{6}$$

$$\frac{\partial \mathbf{u}}{\partial \tau} + (\mathbf{u} - \mathbf{w}) \cdot \nabla \mathbf{u} = -\frac{\rho_{\text{f}}}{\rho_{\text{hnf}}} \nabla P + \left(\frac{\rho_{\text{f}}}{\rho_{\text{hnf}}}\right)\left(\frac{\mu_{\text{hnf}}}{\mu_{\text{f}}}\right) Pr \nabla^2 \mathbf{u} + \frac{(\rho\beta)_{\text{hnf}}}{\rho_{\text{hnf}}\beta_{\text{f}}} PrRaT \tag{7}$$

$$\frac{\partial T}{\partial \tau} + (\mathbf{u} - \mathbf{w}).\nabla T = \frac{\alpha_{\text{hnf}}}{\alpha_{\text{f}}} \nabla^2 T \tag{8}$$

In Eq. (7), the dimensional parameters Pr and Ra are the contractions of the Prandtl number and the Rayleigh number. The nanofluid properties represented in the above equations, including the effective density ρ_{hnf} [57] and the thermal expansion coefficient $(\rho\beta)_{\text{hnf}}$ [57], are defined, respectively, as follows:

$$\rho_{\text{hnf}} = \rho_{\text{f}}(1 - \varphi_{\text{hnp}}) + \rho_{\text{Al}_2\text{O}_3}\varphi_{\text{Al}_2\text{O}_3} + \rho_{\text{Cu}}\varphi_{\text{Cu}} \tag{9}$$

$$(\rho\beta)_{\text{hnf}} = (1 - \varphi_{\text{hnp}})(\rho\beta)_{\text{f}} + \varphi_{\text{Al}_2\text{O}_3}(\rho\beta)_{\text{Al}_2\text{O}_3} + \varphi_{\text{Cu}}(\rho\beta)_{\text{Cu}} \tag{10}$$

so that $\varphi_{\text{hnp}} = \varphi_{\text{Al}_2\text{O}_3} + \varphi_{\text{Cu}}$.

Also, in Eq. (8), $\alpha_{\text{hnf}} = k_{\text{hnf}}/(\rho c_{\text{p}})_{\text{hnf}}$ is the thermal diffusivity of the hybrid nanofluid. The heat capacity of the hybrid nanofluid is calculated as follows:

$$\left(\rho c_{\text{p}}\right)_{\text{hnf}} = \left(1 - \varphi_{\text{hnp}}\right)\left(\rho c_{\text{p}}\right)_{\text{f}} + \varphi_{\text{Al}_2\text{O}_3}\left(\rho c_{\text{p}}\right)_{\text{Al}_2\text{O}_3} + \varphi_{\text{Cu}}\left(\rho c_{\text{p}}\right)_{\text{Cu}} \tag{11}$$

In addition, if the thermal conductivity of the hybrid nanofluid is defined by the classical Maxwell [58] and Bruggeman [59] models, the following modified relations are obtained:

The classical Maxwell model [58]:

$$\frac{k_{\text{hnf}}}{k_{\text{f}}} = \frac{k_{\text{hnp}} + 2k_{\text{f}} - 2\varphi_{\text{hnp}}\left(k_{\text{f}} - k_{\text{hnp}}\right)}{k_{\text{hnp}} + 2k_{\text{f}} + \varphi_{\text{hnp}}\left(k_{\text{f}} - k_{\text{hnp}}\right)} \tag{12}$$

Table 1 Thermophysical properties of the components of Cu–Al_2O_3/water [55, 56]

Physical properties	Water	Cu	Al_2O_3
c_{p}/J kg^{-1} K^{-1}	4179	385	765
k/W m^{-1} K^{-1}	0.613	401	40
α/m^2 s^{-1}	1.47×10^{-7}	1.11×10^{-4}	131.7×10^{-7}
β/K^{-1}	21×10^{-5}	1.67×10^{-5}	0.85×10^{-5}
ρ/kg m^{-3}	997.1	8933	3970
μ/kg m^{-1} s^{-1}	8.9×10^{-4}	–	–

The classical Bruggeman model [59]:

$$k_{\mathrm{hnf}} = \frac{1}{4}\left[(3\varphi_{\mathrm{hnp}} - 1)k_{\mathrm{hnp}} + (2 - 3\varphi_{\mathrm{hnp}})k_{\mathrm{f}}\right] + \frac{k_{\mathrm{f}}}{4}\sqrt{\Delta} \quad (13)$$

$$\Delta = \left[(3\varphi_{\mathrm{hnp}} - 1)^2\left(\frac{k_{\mathrm{hnp}}}{k_{\mathrm{f}}}\right) + (2 - 3\varphi_{\mathrm{hnp}})^2 + 2\left(2 + 9\varphi_{\mathrm{hnp}} - 9\varphi_{\mathrm{hnp}}^2\right)\left(\frac{k_{\mathrm{hnp}}}{k_{\mathrm{f}}}\right)\right] \quad (14)$$

In both of the above relations, k_{hnp} is defined as

$$k_{\mathrm{hnp}}\varphi_{\mathrm{hnp}} = k_{\mathrm{Al_2O_3}}\varphi_{\mathrm{Al_2O_3}} + k_{\mathrm{Cu}}\varphi_{\mathrm{Cu}} \quad (15)$$

It is necessary to say that as the volume fraction of Cu is equal to zero, all equations and relations considered for the Cu–Al_2O_3/water hybrid nanofluid are correct for the Al_2O_3/water nanofluid.

The comparison between the values of thermal conductivity resulting from the above-mentioned relations for the Cu–Al_2O_3/water hybrid nanofluid, and the experimental values presented by [36], show that the Maxwell and Bruggeman relations cannot estimate the correct values of thermal conductivity of the Cu–Al_2O_3/water hybrid nanofluid. So, it seems that it is appropriate to continue the solution process based on the experimental values of the thermal conductivity. On the other hand, the accuracy of the classical models used to get the viscosity of the nanofluid is examined for the Cu–Al_2O_3/water hybrid nanofluid. Here, there are three classical models that are mentioned as follows:

Einstein model [60]:

$$\frac{\mu_{\mathrm{hnf}}}{\mu_{\mathrm{f}}} = 1 + k_{\mu 1}\varphi_{\mathrm{hnp}} \quad (16)$$

Brinkman model [61]:

$$\frac{\mu_{\mathrm{hnf}}}{\mu_{\mathrm{f}}} = \frac{1}{\left(1 - \varphi_{\mathrm{hnp}}\right)^{2.5}} \quad (17)$$

Batchelor model [62]:

$$\frac{\mu_{\mathrm{hnf}}}{\mu_{\mathrm{f}}} = 1 + k_{\mu 1}\varphi_{\mathrm{hnp}} + k_{\mu 2}\varphi_{\mathrm{hnp}}^2 \quad (18)$$

where $k_{\mu 1}$ is 2.5. Also, $k_{\mu 2}$ describes the deviation from the very dilute limit of the suspension. It can be seen from Fig. 2b that the classical models cannot predict the correct values of the viscosity of the Cu–Al_2O_3/water hybrid nanofluid. In addition, it is observed that the underestimation of the viscosity results from utilizing the classical models, in which the viscosity increases as the volume fractions of the nanoparticles Cu and Al_2O_3 increase. Therefore, in the present study, we utilize the experimental values of the viscosity and the thermal conductivity available in the literature [46] and which are represented in Table 2.

The boundary conditions can be rewritten in dimensionless form as follows:

On all the external walls of the cavity $T = 0$ and $u = v = 0$ (19a)

On the oscillating cylinder $T = 1$ (19b)

On the oscillating cylinder $u = 0$ and $v = \frac{\mathrm{d}y}{\mathrm{d}t} = 2A\pi f\cos(2\pi f\tau)$, $A = A^*/L$ (19c)

The non-dimensional steady-state solution for a cavity with a fixed cylinder at its center is considered as the initial condition. It should be noted that the sinusoidal function in the non-dimensional thermal boundary condition appearing as $2\pi f\tau$ can be related with that of $f = \omega L^2/\alpha_{\mathrm{f}}$. Also, it should be noted that the period of oscillation T_{p} is the reverse of the frequency such that $T_{\mathrm{p}} = 1/f$.

The local Nusselt number along the isothermal walls at the dimensional time τ is calculated as:

$$Nu_{\mathrm{local}} = -\frac{k_{\mathrm{hnf}}}{k_{\mathrm{f}}}\left(\frac{\partial T}{\partial n}\right)_{\tau} \quad (20)$$

where n refers to the normal direction to the walls. The average Nusselt number at the time τ Nu_{avg} is obtained by integrating the local Nusselt number Nu_{local}.

$$Nu_{\mathrm{avg}} = \frac{1}{W_0}\int_0^{W_0} Nu_{\mathrm{local}}\mathrm{d}S \quad (21)$$

In the above relation, W_0 is the length of the hot cylinder. The average temperature inside the whole cavity can be calculated as

$$T_{\mathrm{avg}} = \frac{\int_{\bar{V}} T_{\mathrm{local}}\mathrm{d}\bar{V}}{\int_{\bar{V}}\mathrm{d}\bar{V}} \quad (22)$$

Finally, the stream function ψ describing the motion of the fluid flow is expressed as follows:

$$u = \frac{\partial\psi}{\partial y}, \quad v = -\frac{\partial\psi}{\partial x} \quad (23)$$

The solution procedure, grid independence test and validation

The nonlinear and coupled Eqs. (6)–(8) with the boundary conditions imposed in Eq. (19) are solved by the Galerkin weighted residual finite element numerical method. Details of this method have been explained completely in [63]. A non-uniform unstructured moving grid with triangular

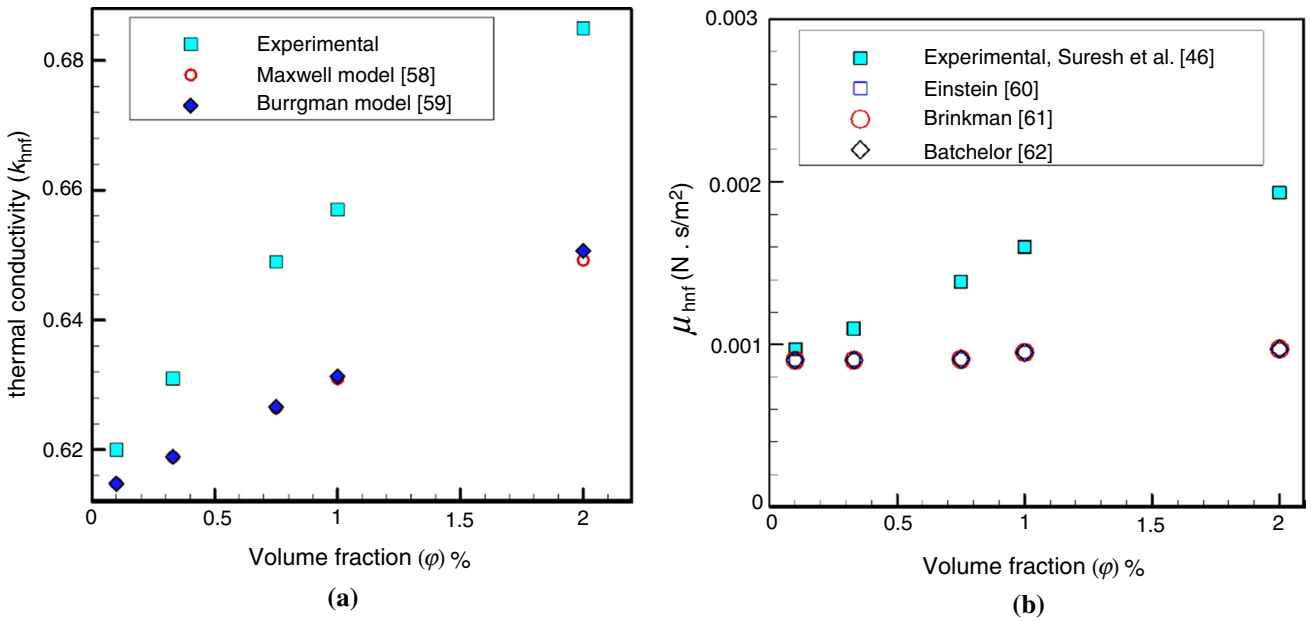

Fig. 2 **a** Thermal conductivity of Cu–Al_2O_3/water hybrid nanofluid with experimental study of [46] and **b** dynamic viscosity of Cu–Al_2O_3/water hybrid nanofluid

Table 2 The thermal conductivity and dynamic viscosity used for both the nanofluid Al_2O_3-water and hybrid nanofluid Cu–Al_2O_3 [46]

φ_{hnp}/%	φ_{Cu}/%	$\varphi_{Al_2O_3}$/%	k_{nf}/W m^{-1} K^{-1}	μ_{nf}/kg m^{-1} s^{-1}	k_{hnf}/W m^{-1} K^{-1}	μ_{hnf}/kg m^{-1} s^{-1}
0.1	0.0038	0.0962	0.614055	0.0009041	0.619982	0.000972
0.33	0.0125	0.3175	0.6190041	0.0009049	0.63098	0.001098
0.75	0.0285	0.7215	0.6309797	0.0009098	0.649004	0.001386
1	0.038	0.9620	0.6437496	0.0009519	0.657008	0.001602
2	0.0759	1.9241	0.6571916	0.0009720	0.684992	0.001935

elements is utilized to discretize the computational domain. Further, in order to increase simulation accuracy, the boundary layer mesh is used close to the solid boundaries. The motion of the mesh was calculated based on the solution of the Laplace equation in the form of $\partial^2 X/\partial x^{2-} + \partial^2 Y/\partial y^2 = 0$ where X and Y denote the deformed positions of the mesh and x and y denote the original positions (underformed). The boundaries of the cylinder are prescribed to the known motion, and hence, the motion of the cylinder would be a Dirichlet boundary condition for the Laplace equation. The boundaries of the cavity are also considered as Dirichlet boundaries with zero displacement. More numerical details can be found in [64, 65]. Due to the important effects of moving fluid and coupling of the flow and heat transfer, adopting sufficient time step is an important issue. In the present study, an automatic time-step procedure is adopted. The free time-step Backward Differentiation Formula in the form of an implicit time-step method is utilized. The order of Backward Differentiation Formula was set variable with the maximum and minimum of 1 and 2, respectively. By interpolating between the accuracy of the previous time steps, the Backward Differentiation Formula solver and automatically selects an appropriate computational time-step to maintain with the adequate accuracy and time convergence of the calculations. Details of the Backward Differentiation Formula scheme can be found in [66, 67].

Before starting the calculations, in order to evaluate the solution sensitivity to the number of elements, a grid independence test is performed. The independence grid test is done based on no significant changes in the Nusselt number on the cylinder surface. The grid sensitivity is carried out for the fixed parameters $A = 0.1$, $f = 1$, $Ra = 10^6$, $Pr = 6.2$ and $\varphi_{hnp} = \varphi_{Al_2O_3} = 0$. Figure 3 shows the grid used to discretize the domain. As shown in Fig. 4, a grid of 24,251 is appropriate to continue the calculations.

A comparison between the present results and the results in the literature has been drawn to explore the accuracy of the modeling of the present problem and the numerical method used to obtain the results. First, the results obtained by this investigation are evaluated with the results represented by Kim et al. [3]. They studied a cold outer square

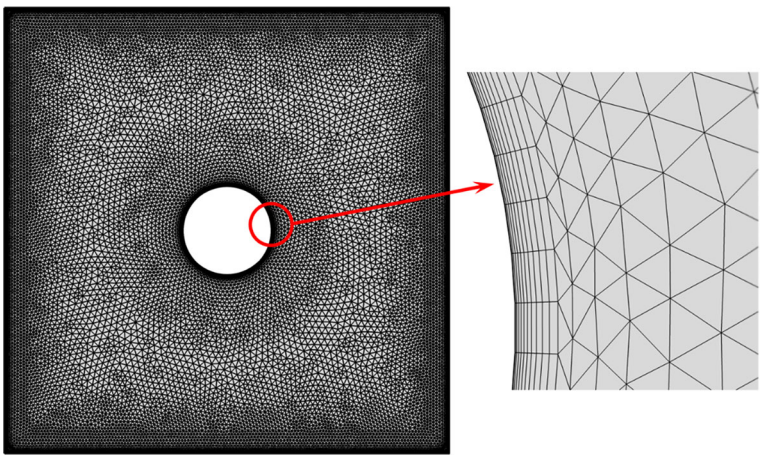

Fig. 3 Grid used to discretize the domain

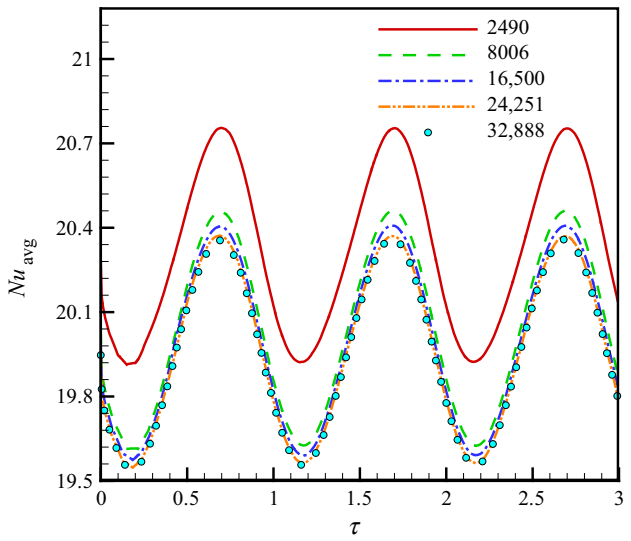

Fig. 4 The average Nusselt number Nu_{avg} on the cylinder surface versus dimensional time in different meshes at $Ra = 10^6$, $A = R$, $f = 1$, $\varphi = 0$

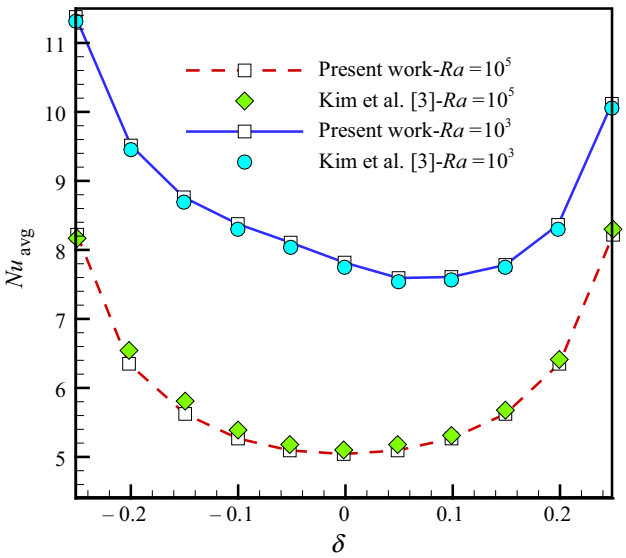

Fig. 5 Comparison of the average Nusselt numbers on the cylinder surface computed in the present work and those reported in Kim et al. [3]

cavity with an inner cylindrical heater whose vertical location can change. Figure 5 displays the variations of Nu_{avg} according to vertical locations of the hot cylinder δ for Ra equal to 10^3 and 10^5 with $Pr = 0.7$ and $R/L = 0.2$. Obviously, an excellent agreement exists between the present results and the work carried out by Kim at el. [3]. This confirms the validity of the modeling and simulation of the present study.

Secondly, the results obtained from this work are compared with the experimental and numerical results of the case study investigated by Cesini et al. [1]. They carried out the numerical and experimental analysis of natural convection of a horizontal hot cylinder in a rectangular enclosure, for which the length of the cavity and the diameter of the cylinder have been considered constant while the width of the cavity is variable. In their cavity, the ratio of the length of the cavity to the diameter of the cylinder is 4.07. Here, the aspect ratio is defined as the width to the diameter and has been chosen to be 2.1. It is worth mentioning that they defined the Rayleigh number based on the diameter of the cylinder D such that $Ra = g\beta(T_H^* - T_C^*)D^3/\nu\alpha$. As Fig. 6 shows, the same trends of the local Nusselt number distribution along the cylinder surface are obtained for the present work and those published by Cesini et al. [1], which also confirms the validity of the present study.

Third, the results of the present method are compared with the results reported by Kahveci [14]. In his study, a simple inclined square cavity has been considered, filled with different types of nanofluids. In this comparison, it is considered that the vertical cavity is filled with Al_2O_3 nanofluid. It should be noted that in the case of a simple cavity, the Rayleigh number is defined based on the size of

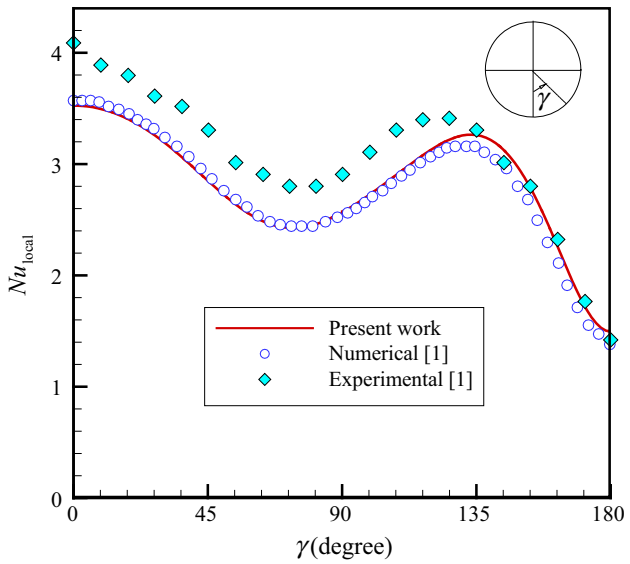

Fig. 6 The local Nusselt distribution along the cylinder surface obtained from [1] and the present work at $Ra = 3.4 \times 10^3$

the cavity (L). A comparison between the results of the present study and those reported by Kahveci [14] is performed in Fig. 7 for different volume fractions of alumina nanoparticles (φ). As shown in Fig. 7, a very high accordance exists between the results published by Kahveci [14] and the results obtained from the present study. This further confirms the accuracy and precision of the simulation.

Finally, as an unsteady case, the results of the present study are compared with the results reported by Xu et al. [68]. In the study by Xu et al. [68], a cavity with the size of L was divided into two halves by a perfectly thermally conductive rigid partition. The halves next to the hot and cold walls were initially at the temperature of the hot wall and the cold wall, respectively. It is worth mentioning that the dimensionless parameters for the non-dimensional time (τ) which was introduced in [68] are different to that of the present study. In [68], the dimensionless time was introduced as $\tau = t\alpha Ra^{1/2}/L^2$. Following the non-dimensional form of the equation reported in [49], the results of the present work are compared with the results reported by Xu et al. [68] in Fig. 8. Figure 8 shows the temperature–time history of a point next to the partition with the non-dimensional coordinate of $x = 0.0083$ and $y = 0.375$. As seen, there is excellent agreement between the results of the present study and the results of Xu et al. [68].

Results and discussion

This section deals with the results obtained from the simulation of the present problem. The effects of the dimensionless parameters such as the Rayleigh number ($10^3 \leq Ra \leq 10^6$), the nanoparticle volume fraction ($0.0 \leq \varphi \leq 0.02$), the oscillation amplitude ($0.5R \leq A \leq 1.5R$), and the frequency ($0.5 \leq f \leq 48$) of the cylinder on the flow and heat transfer characteristics are investigated. The value of the Prandtl number is kept constant at $Pr = 6.2$.

Figure 9 depicts the streamlines and isotherm contours for different values of the volume fraction of a pure fluid, a Cu–Al_2O_3/water hybrid nanofluid and an Al_2O_3/water single nanofluid for $Ra = 10^5$ at $\tau = nT_p + 6T_p/8$, while

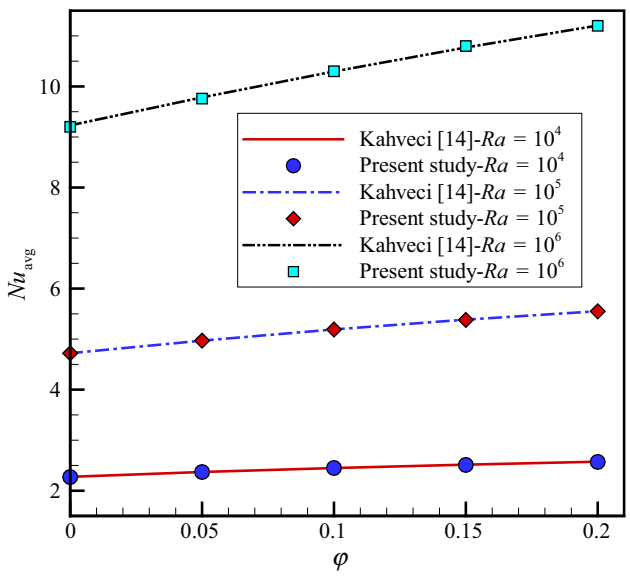

Fig. 7 The variation of Nu_{avg} according to volume fraction of nanoparticles for the different values of Ra resulting from [14] and the present study

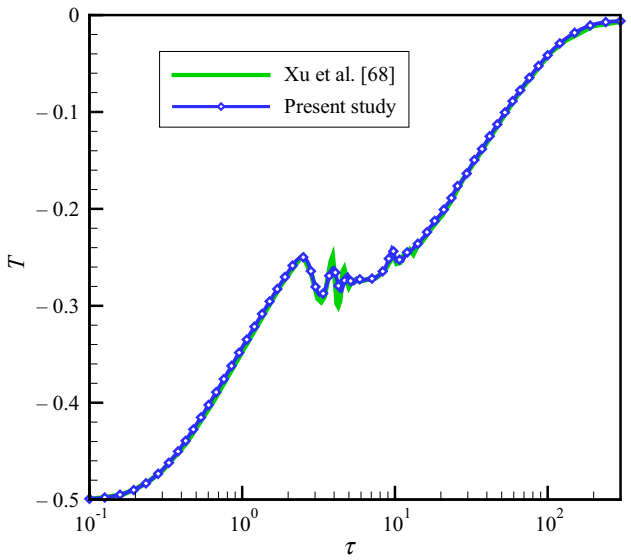

Fig. 8 Comparison of the dimensionless temperature reported by Xu et al. [68] and the present study at the specified point (0.0083, 0.375), in the case of a square cavity divided into two parts by a rigid membrane

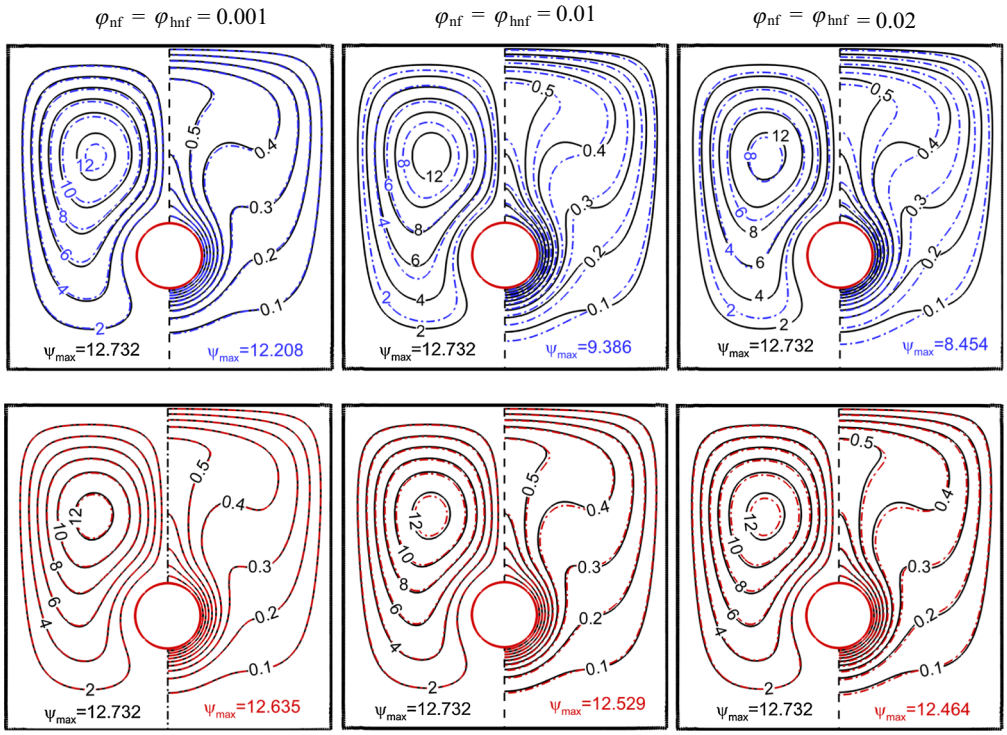

Fig. 9 Exhibition of streamlines and isotherms relating to pure fluid, Al_2O_3 nanofluid and Cu–Al_2O_3 hybrid nanofluid for different values of volume fraction at $Ra = 10^5$, $f = 2$, $A = 1.5R$

f and A are kept fixed at 2 and 1.5R, respectively. In the subfigures available in Fig. 9, the solid lines, dashed lines and dashed-dot lines show the streamlines of the pure fluid, the Al_2O_3/water single nanofluid and the Cu–Al_2O_3/water hybrid nanofluid, respectively.

The results illustrate that the presence of the Al_2O_3 and the Cu–Al_2O_3 nanoparticles decreases the strength of the fluid flow at $Ra = 10^5$, $f = 2$, and $A = 1.5R$. Moreover, it can be seen that the reduction of the strength of the fluid flow due to the simultaneous presence of Cu and Al_2O_3 nanoparticles is much greater than that for the Al_2O_3 nanoparticles. This occurs due to the fact that increasing the viscosity of the hybrid nanofluid due to the simultaneous presence of Cu and Al_2O_3 nanoparticles is extremely larger than increasing the other thermophysical properties, especially the thermal conductivity. In fact, the resistance of the fluid flow becomes stronger against the buoyancy force as the dynamic viscosity of the hybrid nanofluid increases. The maximum reductions in the strength of the flow occur when ψ_{max} is equal to 2.1 and 33.6 percent for the single nanofluid and the hybrid nanofluid, respectively, while φ is equal to 0.02. Furthermore, it is observed that the governing streamline patterns do not change with the presence of Cu–Al_2O_3 and Al_2O_3 nanoparticles; however, the nanoparticles can dramatically change the initial locations of the streamlines of the Cu–Al_2O_3 hybrid nanofluid, especially for $\varphi_{hnf} = 0.01$ and 0.02.

The corresponding isotherms of the streamlines shown in Fig. 9 for both the single nanofluid and the hybrid nanofluid illustrate that the presence of Al_2O_3 nanoparticles does not affect the contour lines. However, utilizing Cu–Al_2O_3 nanoparticles changes the location of the contour lines for the volume fractions $\varphi_{hnf} = 0.01$ and 0.02. In fact, the curvature of the isotherm lines reduces with the reduction of the strength of the fluid flow due to the presence of the Cu–Al_2O_3 nanoparticles.

A set of subfigures is shown in Fig. 10I, II displaying the streamlines and isotherms relating to the pure fluid and the Cu–Al_2O_3 hybrid nanofluid for a volume fraction $\varphi_{hnf} = 0.02$ during a period of oscillation for $Ra = 10^3$ and $Ra = 10^5$, while $A = R$ and $f = 4$. It is worth mentioning that the considered period to exhibit the streamlines and isotherms is sufficiently far from the initial conditions so that the presented results are independent from the initial conditions. Similarly to Fig. 9, it can be seen that the volume fraction $\varphi_{hnf} = 0.02$ of Cu and Al_2O_3 hybrid nanoparticles strongly reduces the strength of the fluid flow. As is obvious, the maximum reduction of the strength of the flow occurs for the case in which ψ_{max} is equal to 56 and 35.1% for $Ra = 10^3$ and 10^5, respectively. Accordingly, the initial location of the streamlines is greatly changed, particularly at high values of ψ. In general, it can be seen that the strength of the fluid flow decreases as the hot cylinder oscillates upward. This phenomenon can be

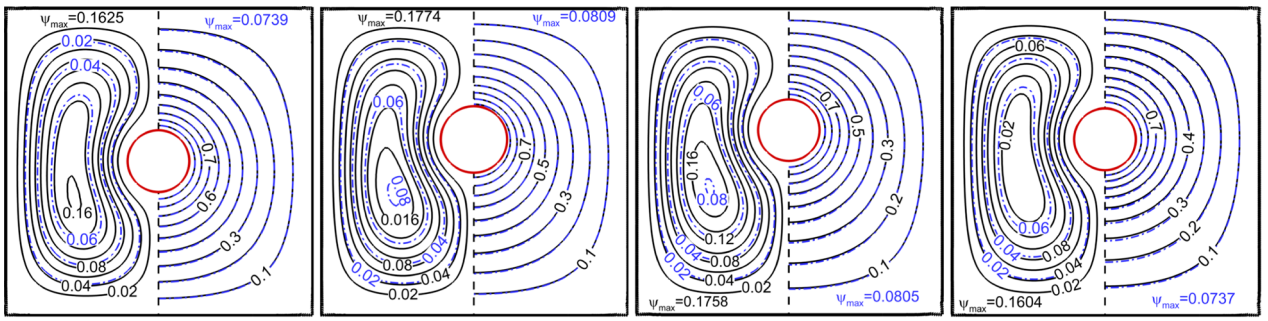

nT_p $nT_p + T_p/8$ $nT_p + 2T_p/8$ $nT_p + 3T_p/8$

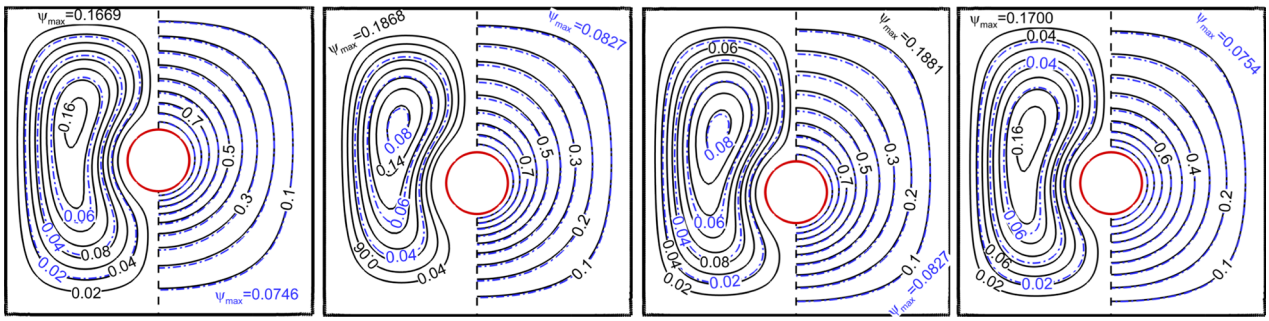

$nT_p + 4T_p/8$ $nT_p + 5T_p/8$ $nT_p + 6T_p/8$ $nT_p + 7T_p/8$

(I) : $Ra = 10^3$

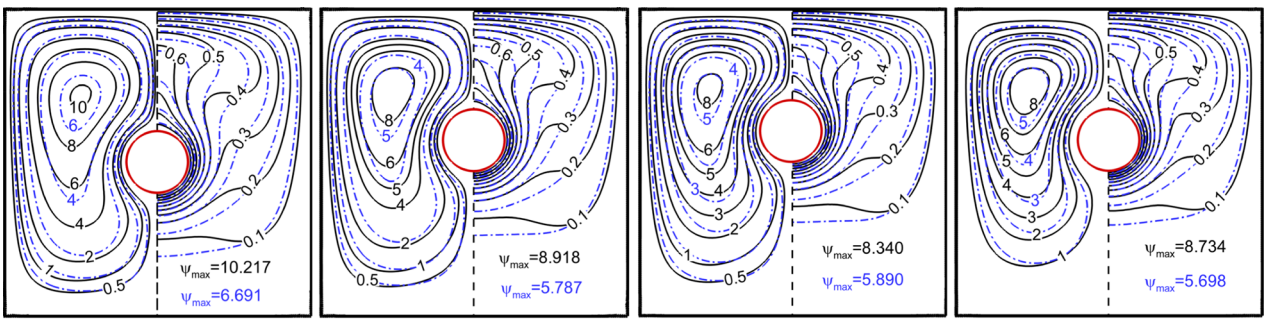

nT_p $nT_p + T_p/8$ $nT_p + 2T_p/8$ $nT_p + 3T_p/8$

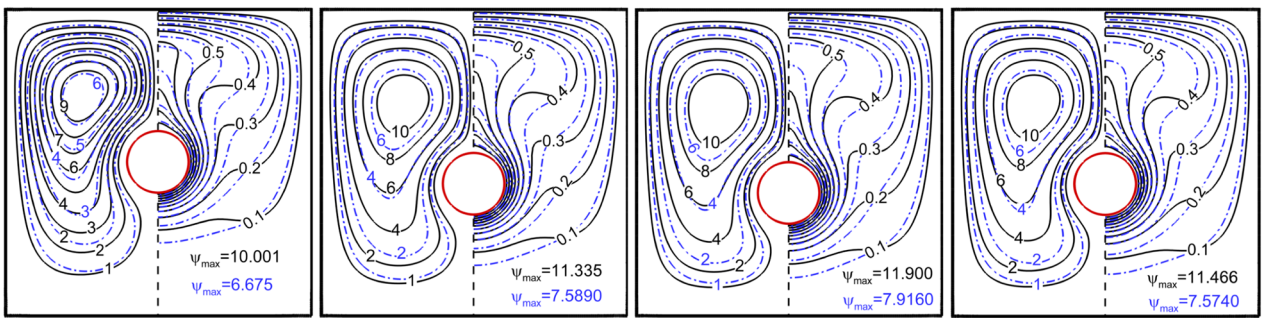

$nT_p + 4T_p/8$ $nT_p + 5T_p/8$ $nT_p + 6T_p/8$ $nT_p + 7T_p/8$

(II) : $Ra = 10^5$

◀**Fig. 10** Exhibition of streamlines and isotherms relating to pure fluid and hybrid nanofluid with volume fraction $\varphi_{hnf} = 0.02$ during a period of oscillation at **I** $Ra = 10^3$ and **II** $Ra = 10^5$ for $A = R$, $f = 4$

explained due to the decrease in the temperature gradient between the hot cylinder and the adjacent fluid when the hot cylinder moves upward in the direction of the top wall. In contrast, the strength of the fluid flow augments as the oscillating cylinder moves downward in the direction of the bottom wall. It is noteworthy that at $Ra = 10^3$, the core of the recirculating vortex inside the cavity is dislocated as the cylinder moves toward the upward or downward directions, while those formed inside the cavity with $Ra = 10^5$ are always in the upper half of the cavity. This is due to the fact that, when the Rayleigh number is low ($Ra = 10^3$) and $f = 4$, the movement of the hot cylinder is dominant compared to the convection.

Figure 11 illustrates the distributions of the streamlines and isotherms related to the pure fluid and the Al_2O_3 nanofluid at the dimensionless time $\tau = nT_p + T_p/8$ for different values of frequencies and for Ra equal to 10^4 and 10^6, in which A and φ are kept constant at R and 0.02, respectively. Clearly, when the value of the Rayleigh number increases from 10^4 to 10^6, the strength and the size of the vortices increase considerably, as a result of the increase in the buoyancy force. Additionally, an increase in the buoyancy force causes a decline in the thickness of the thermal boundary layer around the surface of the cylinder. Moreover, when $Ra = 10^4$, the patterns of the streamlines and the isotherms are generally similar to those associated with $Ra = 10^3$, as displayed in Fig. 10I.

In addition, as the frequency increases, the strength of the fluid flow augments. This occurs due to the decrease in the thickness of the boundary layer around the oscillating cylinder. Furthermore, it is observed that when $Ra = 10^4$, the core of the recirculating vortex moves downward as the frequency increases. While the value of Ra is equal to 10^6, the location of the center of the vortices remains constant with increasing values of the frequency. In this case, the two vortices formed inside the cavity approach each other as a result of the increase in the frequency, and finally a unique vortex is formed at $f = 20$. Although augmentation in the values of the frequency does not change the general shape of the isotherm patterns, it can, however, dislocate their initial locations.

As the drawn streamline values in Fig. 11 show that a volume fraction of 2% of Al_2O_3 nanoparticles decreases and increases the strength of the fluid flow at $Ra = 10^4$ and $Ra = 10^6$, respectively. Figure 12 displays the patterns of the streamlines and the isotherms related to the pure fluid and the hybrid nanofluid with $\varphi = 0.02$ for different values of A while $Ra = 10^5$ and $f = 8$. The top and bottom rows

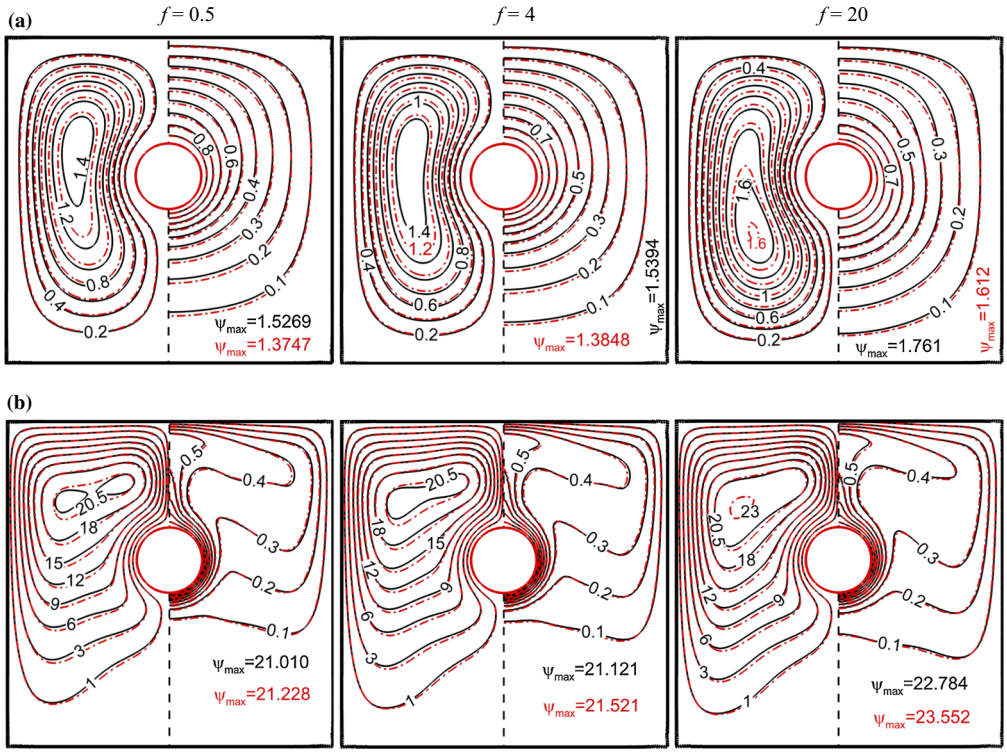

Fig. 11 Exhibition of streamlines and isotherms relating to pure fluid and Al_2O_3 nanofluid for different values of frequency at **a** $Ra = 10^4$ and **b** $Ra = 10^5$ for $A = R$ and $\varphi_{nf} = 0.02$ when $\tau = n\mathrm{Tp} + \mathrm{Tp}/8$

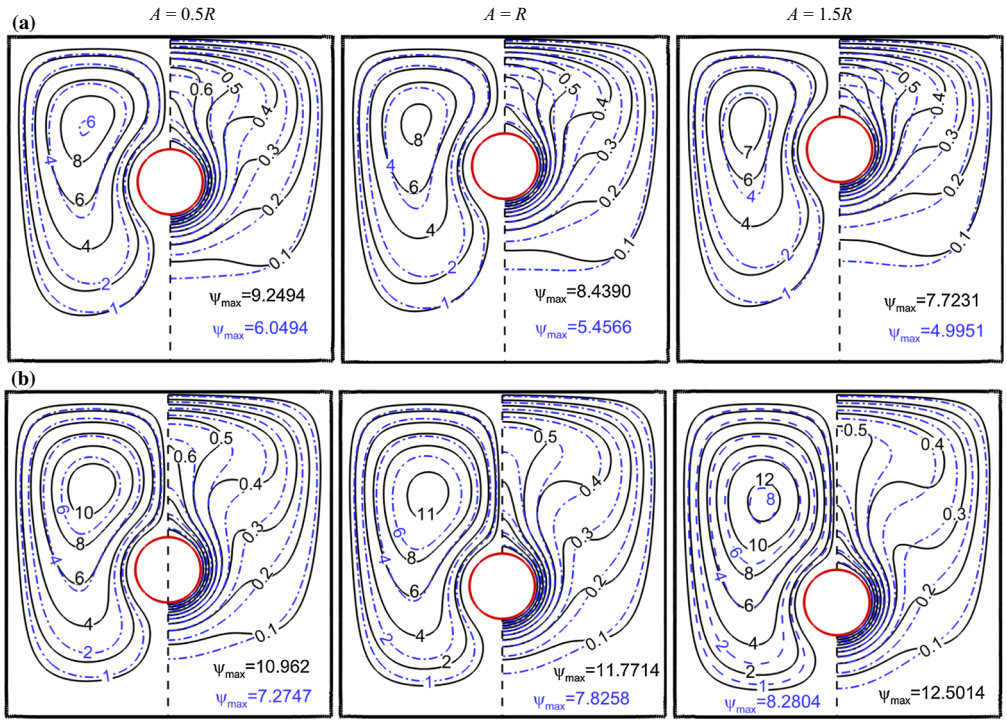

Fig. 12 Exhibition of streamlines and isotherms relating to pure fluid and Cu–Al_2O_3 hybrid nanofluid at two different location of the cylinder for different values of A at $Ra = 10^5$, $f = 8$ and $\varphi_{hnf} = 0.02$; **a** the cylinder is at the minimum distance from the top and **b** the cylinder is at the minimum distance from the bottom

show the location of the inner cylinder at the nearest distance from the top and bottom walls, respectively. As shown, increasing the oscillating amplitude results in decreasing and increasing the ψ_{max} which represents the strength of the fluid flow at the highest and lowest location of the cylinder in the cavity. This is due to the fact that when the oscillating cylinder becomes closer to the top wall, the temperature gradient reduces. In contrast, when the hot cylinder becomes closer to the bottom wall, the temperature gradient increases as a result of the increase in amplitude. In addition, it is observed that the lines of the isotherms near the top wall of the cavity are accumulated and compressed when the hot cylinder becomes closer to that wall as a result of increasing the amplitude.

Figure 13 illustrates the variations of the surface average Nusselt number of the hot oscillating cylinder for the cases of pure fluid, nanofluid and hybrid nanofluid versus the dimensionless time τ for different values of A at $Ra = 10^3$ and $Ra = 10^6$, when the frequency has low and high values of $f = 1$ and 48, respectively. The comparison of the distribution of the Nusselt number as a function of the dimensionless time between the graphs relating to $Ra = 10^3$ and 10^6 show a phase difference between them, so that the average Nusselt number increases and decreases for $Ra = 10^3$ and 10^6, respectively, when the hot cylinder oscillates upward in the direction of the top wall. When the value of the Rayleigh number is low ($Ra = 10^3$), the average Nusselt number increases as the hot oscillating cylinder moves upward. The increasing trend of Nu_{avg} continues until the hot cylinder reaches its minimum distance from the top wall. After that, when the oscillating cylinder goes back vertically downward along the square centerline, the average Nusselt number is reduced until it reaches its relative minimum value when the cylinder moves downward passing from its initial location. Afterward, as the cylinder is inserted into the bottom half of the cavity, the average Nusselt number augments again until it reaches its maximum value at the lowest location of the cylinder. Finally, it is observed that the heat transfer rate continues to decrease until reaching an absolute minimum value.

In addition, for low and high frequencies at both $Ra = 10^3$ and 10^6, as the amplitude of the oscillation increases, the amplitude of variations of Nu_{avg} augments. It is worth mentioning that at the low frequency $f = 1$ and $Ra = 10^3$, increasing the amplitude of the oscillation results in an augmentation in the minimum value of Nu_{avg} during one period, while in the other cases, this increase in the amplitude of oscillation causes a decrease in the Nu_{avg} minimum value. On the other hand, at the high Rayleigh number $Ra = 10^6$, it can be seen that the minimum and maximum heat transfer rates occur at the lowest and highest distances from the top wall of the cavity. Moreover, the results indicate that when the Rayleigh number value is

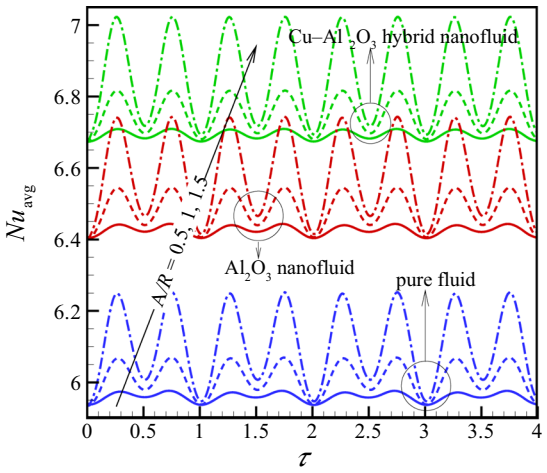

Nanofluid and hybrid nanofluid for $f = 1$ and $Ra = 10^3$

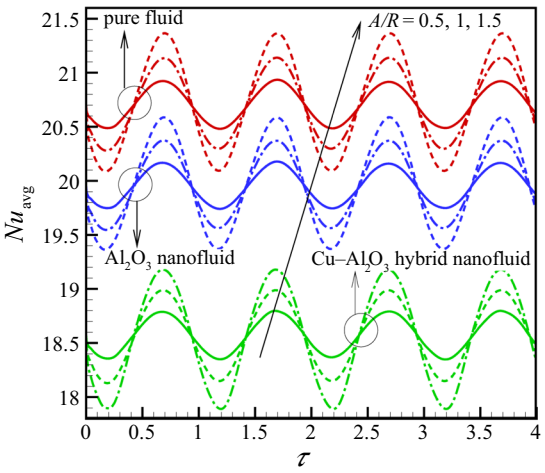

Nanofluid and hybrid nanofluid for $f = 1$ and $Ra = 10^6$

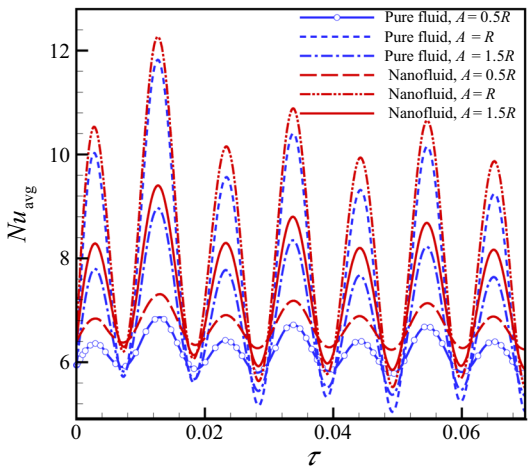

Nanofluid for $f = 48$ and $Ra = 10^3$

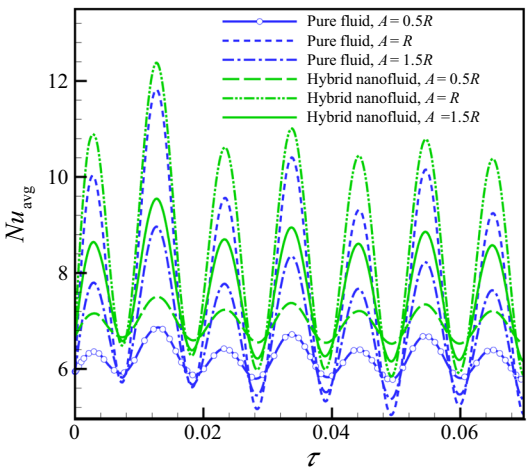

Hybrid nanofluid for $f = 48$ and $Ra = 10^3$

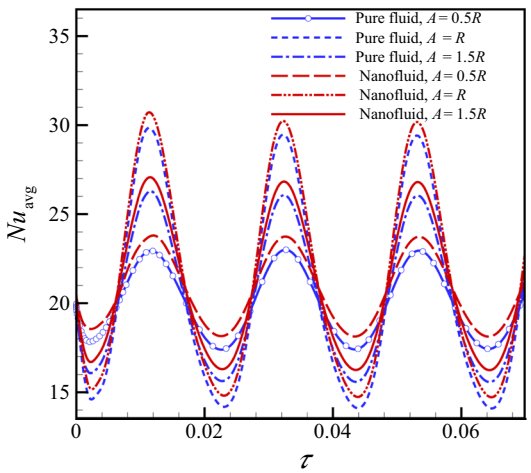

Nanofluid for $f = 48$ and $Ra = 10^6$

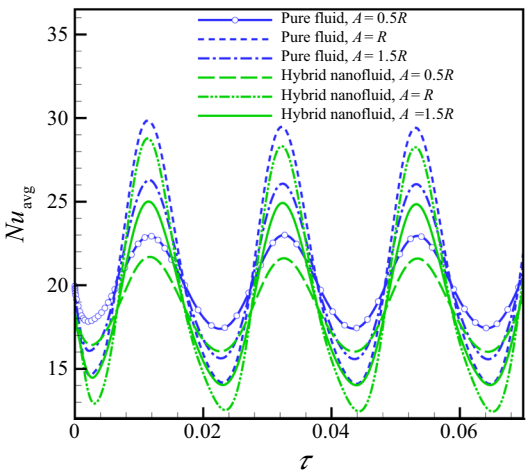

Hybrid nanofluid for $f = 48$ and $Ra = 10^6$

Fig. 13 The variations of the Nusselt number around the oscillation cylinder versus the dimensionless time for the different values of A at Ra values of $Ra = 10^3$ and 10^6 for the low and high frequency 1 and 48, respectively

Table 3 A comparison of the values obtained for time-averaged Nusselt number among pure fluid, nanofluid, and hybrid nanofluid at one oscillation period for $A = R$

φ (%)	$f = 1$				$f = 48$			
	$Ra = 10^3$		$Ra = 10^6$		$Ra = 10^3$		$Ra = 10^6$	
	NF	HNF	NF	HNF	NF	HNF	NF	HNF
0.0	6.013	6.013	19.968	19.968	6.776	6.776	21.460	21.460
0.1	6.029	6.086	19.941	19.788	6.793	6.848	21.435	21.285
0.33	6.082	6.197	20.063	19.561	6.846	6.957	21.557	21.064
0.75	6.206	6.379	20.343	19.062	6.973	7.142	21.837	20.572
1	6.335	6.461	20.469	18.684	7.105	7.215	21.965	20.209
2	6.484	6.753	20.717	18.576	7.259	7.514	22.213	20.110

Table 4 The values obtained for time-averaged Nusselt number at the different values of A for Ra value of $Ra = 10^3$ and $Ra = 10^6$ at low and high value of $f = 1$ and 48, respectively

A/R	$f = 1$						$f = 48$					
	$Ra = 10^3$			$Ra = 10^6$			$Ra = 10^3$			$Ra = 10^6$		
	PF	NF	HNF	PF	NF	HNF	PF	NF	HNF	PF	NF	HNF
0.5	5.960	6.427	6.694	19.957	20.705	18.574	6.216	6.672	6.935	20.651	21.406	19.285
1.0	6.013	6.484	6.753	19.968	20.717	18.576	6.776	7.259	7.514	21.460	22.213	20.110
1.5	6.109	6.586	6.859	19.980	20.729	18.565	7.563	8.072	8.341	22.418	23.165	21.091

low ($Ra = 10^3$), the presence of Al_2O_3 and Cu–Al_2O_3 nanoparticles augments Nu_{avg}, while at $Ra = 10^6$, the presence of Cu–Al_2O_3 nanoparticles causes a decline in the values of Nu_{avg}. In fact, at a low Rayleigh number value, the conduction heat transfer mechanism is dominant, and thus, the changing of the viscosity does not have a significant effect on the heat transfer rate. However, an increase or a decrease in thermal conductivity can strongly affect heat transfer. Additionally, whereas when Ra equals 10^6, a significant increase in the dynamic viscosity, as a resistance force, can reduce the mobility of the fluid. Thus, at this value of Ra, the Al_2O_3 nanoparticles with $\varphi_{Al_2O_3} = 0.02$ increase Nu_{avg} due to the augmentation of the mobility and the thermal conductivity of fluid flow.

A comparison of the time-averaged Nusselt number Nu_{avg_t} during a period of oscillation between the Al_2O_3–water nanofluid and Cu–Al_2O_3/water hybrid nanofluid, for different values of φ at $Ra = 10^3$ and 10^6, and the low and high frequencies of $f = 1$ and 48, respectively, is presented in Table 3. In the table, the symbols PF, NF and HNF refer to the pure fluid, Al_2O_3 nanofluid and the Cu–Al_2O_3 hybrid nanofluid, respectively. The data presented in Table 3 indicate that for $Ra = 10^6$ at both frequencies, the Nu_{avg_t} is decreased slightly by using the value of 0.1 volume fraction of Al_2O_3 nanoparticles compared to the pure fluid. Moreover, when Ra is equal to 10^6, increasing the volume fraction of the Al_2O_3 and Cu–Al_2O_3 nanoparticles escalates and decreases the Nu_{avg_t}, respectively. On the other hand, when Ra is equal to 10^3, the heat transfer rate during a period of oscillation increases with increasing values of the volume fraction for both types of nanoparticles. Further, the results indicate that an increase in Ra greatly augments the heat transfer rate. Finally, it is observed that the time-averaged Nusselt number can be increased with an increase in frequency.

The effects of the amplitude of the oscillating cylinder A on the time-averaged Nusselt number $Nu_{avg\text{-}t}$ during a period of oscillation at the Ra values of $Ra = 10^3$ and 10^6 for the low and high values of the frequency, $f = 1$ and 48, respectively, are presented in Table 4. Generally, it can be seen that for all the states and types of the fluid, $Nu_{avg\text{-}t}$ increases when A augments. In both cases in which the Ra is equal to 10^3 and 10^6, augmentation in the values of the heat transfer rate is larger for the high frequency $f = 48$ as compared to the low frequency $f = 1$.

Figure 14 illustrates the variations of the average temperature as a function of the dimensionless time (τ) for the different values of the non-dimensional amplitude (A/R). The results are depicted for two cases of $Ra = 10^3$ (the weak buoyancy forces regime) and 10^6 (strong buoyancy forces regime). Two frequency values of $f = 1$ (low) and $f = 48$ (high) are selected for illustration of the results. Obviously, for all the cases presented here, the amplitude

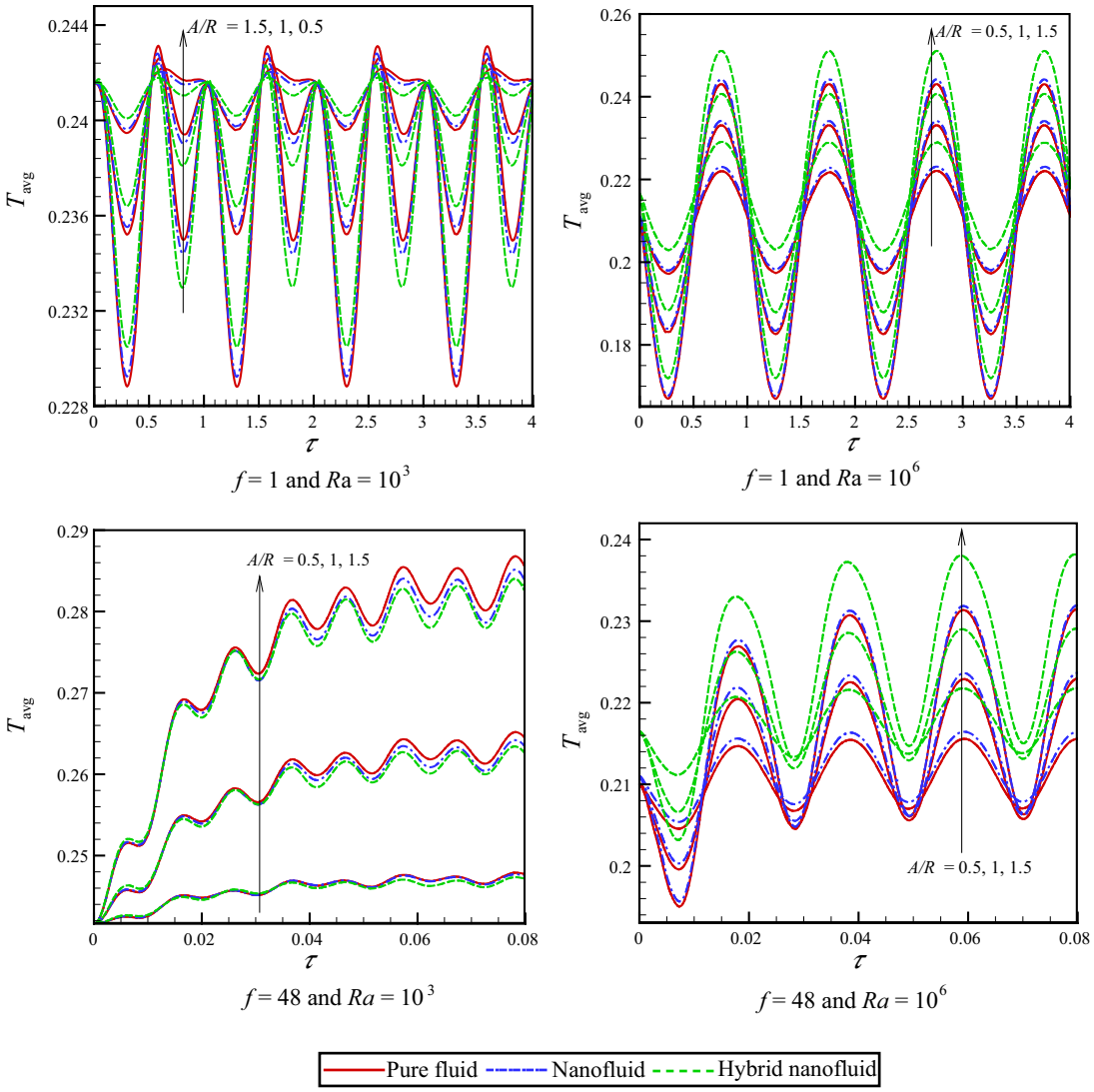

Fig. 14 The variations of the average temperature versus the dimensionless time for the different values of A at Ra values of $Ra = 10^3$ and 10^6 for the low and high frequencies 1 and 48, respectively

of the variation of T_{avg} increases as the amplitude of the cylinder oscillation (A/R) increases.

For both the low and high values of the frequency at $Ra = 10^6$, when the hot oscillating cylinder reaches the upper half of the cavity, the average temperature declines. This is due to the decrease in the heat transfer rate as a result of the reduction in the temperature difference between the hot cylinder and the adjacent fluid. Generally, when Ra is equal to 10^6, the minimum and maximum values of T_{avg} during a period of oscillation occur at the highest and lowest location of the cylinder in the cavity, respectively. On the other hand, for $Ra = 10^3$, the temporal trend of the average temperature related to the low and high values of f is completely different, as shown in Fig. 14. Clearly, at the beginning of the oscillation when $f = 1$, the average temperature reduces until it reaches its own minimum at the highest location of the cylinder in the cavity. After that, T_{avg} begins to reduce as the hot cylinder goes back to the center of the cavity in the direction of the bottom wall. It can be seen that for $Ra = 10^3$ and $f = 1$, the maximum value of T_{avg} occurs when the cylinder moves downward passing from its initial location. Finally, T_{avg} has a relative minimum value at the lowest location of the cylinder in the cavity. When $Ra = 10^3$ and $f = 48$, it is observed that the average temperature increases considerably in the first full oscillation of the cylinder. This is due to the fact that an extreme increase in the heat transfer rate results in a decline in the boundary layer thickness. Moreover, the rate of increase in the average temperature for the next periods reduces, as the number of oscillations of the cylinder augments. When the Rayleigh number is low ($Ra = 10^3$), using Al_2O_3 or Cu–Al_2O_3 nanoparticles

Table 5 The values obtained for time-averaged temperature at the different values of A for Ra values of $Ra = 10^3$ and $Ra = 10^6$ at the low and high value of $f = 1$ and 48, respectively

A/R	$f = 1$						$f = 48$					
	$Ra = 10^3$			$Ra = 10^6$			$Ra = 10^3$			$Ra = 10^6$		
	PF	NF	HNF	PF	NF	HNF	PF	NF	HNF	PF	NF	HNF
0.5	0.241	0.241	0.241	0.210	0.211	0.216	0.246	0.246	0.245	0.211	0.212	0.217
1.0	0.237	0.239	0.239	0.209	0.210	0.215	0.258	0.257	0.257	0.213	0.214	0.218
1.5	0.237	0.237	0.237	0.207	0.208	0.214	0.274	0.273	0.273	0.217	0.217	0.224

with the total volume fraction of $\varphi = 0.02$ shows different trends of behavior for the variation of T_{avg}, depending on the applied frequencies.

In the case of the low frequency of cylinder oscillation, $f = 1$, using Al_2O_3 or Cu–Al_2O_3 as additives can increase the absolute minimum and decrease the maximum values of T_{avg}; on the other hand, both nanoparticle types cause a decline in the relative minimum value of T_{avg}. However, at the high frequency of $f = 48$, using Al_2O_3 or Cu–Al_2O_3 nanoparticles results in the reduction of T_{avg} in the cavity. The graphs plotted for $Ra = 10^6$ show that Cu–Al_2O_3 nanoparticles can increase the average temperature, whereas the Al_2O_3 nanoparticles do not affect the average temperature significantly. In fact, a significant augmentation of T_{avg} comes from the increased dynamic viscosity resulting from the presence of Cu–Al_2O_3 nanoparticles.

The results presented in Table 5 give details of the changes in the time-averaged temperature T_{avg-t} on the basis of the variations of the amplitude at Ra values of $Ra = 10^3$ and $Ra = 10^6$ for the low and high values of the frequency $f = 1$ and 48, respectively. An increase in the amplitude of oscillation causes a decline in the value of the time-averaged temperature when the frequency value is the low $f = 1$; in contrast, when f is equal to 48, the time-averaged temperature augments as the amplitude of oscillation increases. In addition, for both values of the frequency at $Ra = 10^6$, the Al_2O_3 and Cu–Al_2O_3 nanoparticles with $\varphi = 0.02$ augment T_{avg-t} compared to a pure fluid; however, the increase of T_{avg-t} due to the existence of Cu–Al_2O_3 nanoparticles is larger than that for the Al_2O_3 nanoparticles. Finally, it can be concluded that when $Ra = 10^3$ and $f = 1$, the nanoparticles have no effects on T_{avg-t}.

Conclusions

The effects of a Cu–Al_2O_3/water hybrid nanofluid and an Al_2O_3/water nanofluid on the mixed convection inside a square cavity in the presence of a hot oscillation cylinder are investigated. The governing equations are reduced to a non-dimensional form and then solved numerically using the Galerkin finite element method using a non-uniform unstructured moving grid with triangular elements. The effects of several parameters, such as the Rayleigh number Ra, the nanoparticle volume fraction φ, the amplitude of oscillation A, and the period of the oscillation of the cylinder f are studied. The most important observations can be summarized as follows:

- The presence of the Al_2O_3 and Cu–Al_2O_3 nanoparticles causes the strength of the fluid flow to decline for the chosen values of $Ra = 10^5$, $f = 2$ and $A = 1.5R$. However, the reduction resulting from the hybrid nanoparticles is larger than that of the Al_2O_3 nanoparticles. This is due to the fact that the resistance of the fluid flow against the buoyancy force increases because of the greater dynamic viscosity of the hybrid nanofluid.
- As the value of the Rayleigh number increases from 10^4 to 10^6, the strength and the size of the vortices significantly increase, due to the increase in the buoyancy force, which reduces the thickness of the thermal boundary layer around the surface of the cylinder.
- When the oscillating cylinder approaches the top wall, the temperature gradient reduces; in contrast, when the hot cylinder becomes closer to the bottom wall, the temperature gradient augments. Additionally, in the case when the value of the Rayleigh number is low ($Ra = 10^3$), the average Nusselt number augments as the hot oscillating cylinder moves from its initial condition toward the top and bottom walls.
- For low values of the Rayleigh number, the presence of the Al_2O_3 and the Cu–Al_2O_3 nanoparticles causes an increase in the values of the average Nusselt number Nu_{avg}. However, for large values of the Rayleigh number, only the simple Al_2O_3 shows heat transfer enhancement, and the presence of the Cu–Al_2O_3 nanoparticles decreases the values of Nu_{avg}. Furthermore, for low values of the Rayleigh number, as the volume fraction of both types of nanoparticles increases, the heat transfer rate during a period of oscillation increases.
- Increasing the amplitude of the cylinder oscillation does not always enhance the heat transfer, and there are cases of hybrid nanofluid (HNF) in which the heat transfer may decrease.

- Raising the period of the oscillation from $f = 1$ to $f = 48$ results in the enhancement of the heat transfer rate. Therefore, moderate high-frequency oscillations of the cylinder could result in higher heat transfer rate compared to the case of low frequency. This result is valid for all of the cases of pure fluid (PF), nanofluid (NF) and hybrid nanofluid (HNF).

References

1. Cesini G, Paroncini M, Cortella G, Manzan M. Natural convection from a horizontal cylinder in a rectangular cavity. Int J Heat Mass Transf. 1999;42(10):1801–11.
2. Yoon HS, Ha MY, Kim BS, Yu DH. Effect of the position of a circular cylinder in a square enclosure on natural convection at Rayleigh number of 10 7. Phys Fluids. 2009;21(4):047101.
3. Kim B, Lee D, Ha M, Yoon H. A numerical study of natural convection in a square enclosure with a circular cylinder at different vertical locations. Int J Heat Mass Transf. 2008;51(7–8):1888–906.
4. Park Y, Ha M, Yoon H. Study on natural convection in a cold square enclosure with a pair of hot horizontal cylinders positioned at different vertical locations. Int J Heat Mass Transf. 2013;65:696–712.
5. Kang DH, Ha MY, Yoon HS, Choi C. Bifurcation to unsteady natural convection in square enclosure with a circular cylinder at Rayleigh number of 107. Int J Heat Mass Transf. 2013;64:926–44.
6. Doo JH, Mun GS, Ha MY, Seong SY. Thermo-dynamic irreversibility induced by natural convection in square enclosure with inner cylinder. Part-II: effect of vertical position of inner cylinder. Int J Heat Mass Transf. 2016;97:1120–39.
7. Huang Z, Zhang W, Xi G. Natural convection in square enclosure induced by inner circular cylinder with time-periodic pulsating temperature. Int J Heat Mass Transf. 2015;82:16–25.
8. Zhang P, Zhang X, Deng J, Song L. A numerical study of natural convection in an inclined square enclosure with an elliptic cylinder using variational multiscale element free Galerkin method. Int J Heat Mass Transf. 2016;99:721–37.
9. Chamkha AJ, Hussain SH, Abd-Amer QR. Mixed convection heat transfer of air inside a square vented cavity with a heated horizontal square cylinder. Numer Heat Transf A Appl. 2011;59(1):58–79.
10. Hussein AK. Computational analysis of natural convection in a parallelogrammic cavity with a hot concentric circular cylinder moving at different vertical locations. Int Commun Heat Mass Transf. 2013;46:126–33.
11. Butler C, Newport D, Geron M. Natural convection experiments on a heated horizontal cylinder in a differentially heated square cavity. Exp Therm Fluid Sci. 2013;44:199–208.
12. Chamkha AJ, Selimefendigil F, Ismael MA. Mixed convection in a partially layered porous cavity with an inner rotating cylinder. Numer Heat Transf A Appl. 2016;69(6):659–75.
13. Choi SU, Eastman JA. Enhancing thermal conductivity of fluids with nanoparticles. Lemont: Argonne National Lab; 1995.
14. Kahveci K. Buoyancy driven heat transfer of nanofluids in a tilted enclosure. J Heat Transf. 2010;132(6):062501.
15. Garoosi F, Rohani B, Rashidi MM. Two-phase mixture modeling of mixed convection of nanofluids in a square cavity with internal and external heating. Powder Technol. 2015;275:304–21.
16. Ganji D, Malvandi A. Natural convection of nanofluids inside a vertical enclosure in the presence of a uniform magnetic field. Powder Technol. 2014;263:50–7.
17. Abolbashari MH, Freidoonimehr N, Nazari F, Rashidi MM. Analytical modeling of entropy generation for Casson nano-fluid flow induced by a stretching surface. Adv Powder Technol. 2015;26(2):542–52.
18. Sheikholeslami M, Rashidi M, Hayat T, Ganji D. Free convection of magnetic nanofluid considering MFD viscosity effect. J Mol Liq. 2016;218:393–9.
19. Sheikholeslami M. Magnetic field influence on CuO–H2O nanofluid convective flow in a permeable cavity considering various shapes for nanoparticles. Int J Hydrogen Energy. 2017;42(31):19611–21.
20. Sheikholeslami M. CVFEM for magnetic nanofluid convective heat transfer in a porous curved enclosure. Eur Phys J Plus. 2016;131(11):413.
21. Malvandi A. Anisotropic behavior of magnetic nanofluids (MNFs) at film boiling over a vertical cylinder in the presence of a uniform variable-directional magnetic field. Powder Technol. 2016;294:307–14.
22. Makulati N, Kasaeipoor A, Rashidi M. Numerical study of natural convection of a water–alumina nanofluid in inclined C-shaped enclosures under the effect of magnetic field. Adv Powder Technol. 2016;27(2):661–72.
23. Mahian O, Kolsi L, Amani M, Estellé P, Ahmadi G, Kleinstreuer C, Marshall JS, Siavashi M, Taylor RA, Niazmand H, Wongwises S, Hayat T, Kolanjiyil A, Kasaeian A, Pop I. Recent advances in modeling and simulation of nanofluid flows—part I: fundamental and theory. Phys Rep. 2018. https://doi.org/10.1016/j.physrep.2018.11.004.
24. Mahian O, Kolsi L, Amani M, Estellé P, Ahmadi G, Kleinstreuer C, Marshall JS, Taylor RA, Abu-Nada E, Rashidi S, Niazmand H, Wongwises S, Hayat T, Kasaeian A, Pop I. Recent advances in modeling and simulation of nanofluid flows—part II: applications. Phys Rep. 2018. https://doi.org/10.1016/j.physrep.2018.11.003.
25. Malvandi A, Ganji D. Mixed convective heat transfer of water/alumina nanofluid inside a vertical microchannel. Powder Technol. 2014;263:37–44.
26. Sheikholeslami M, Ganji DD. Nanofluid flow and heat transfer between parallel plates considering Brownian motion using DTM. Comput Methods Appl Mech Eng. 2015;283:651–63.
27. Sheikholeslami M. Numerical modeling of nano enhanced PCM solidification in an enclosure with metallic fin. J Mol Liq. 2018;259:424–38.
28. Sheikholeslami M. CuO-water nanofluid free convection in a porous cavity considering Darcy law. Eur Phys J Plus. 2017;132(1):55.
29. Abu-Nada E, Chamkha AJ. Mixed convection flow of a nanofluid in a lid-driven cavity with a wavy wall. Int Commun Heat Mass Transf. 2014;57:36–47.
30. Sheremet MA, Pop I. Conjugate natural convection in a square porous cavity filled by a nanofluid using Buongiorno's mathematical model. Int J Heat Mass Transf. 2014;79:137–45.
31. Sheremet MA, Grosan T, Pop I. Free convection in a square cavity filled with a porous medium saturated by nanofluid using Tiwari and Das' nanofluid model. Transp Porous Media. 2015;106(3):595–610.
32. Garoosi F, Bagheri G, Rashidi MM. Two phase simulation of natural convection and mixed convection of the nanofluid in a square cavity. Powder Technol. 2015;275:239–56.
33. Mansour M, Chamkha A, Bakier M. Magnetohydrodynamic natural convection and entropy generation of a Cu–water nanofluid in a cavity with wall mounted heat source/sink. J Nanofluids. 2015;4(2):254–69.

34. Bondareva NS, Sheremet MA, Oztop HF, Abu-Hamdeh N. Heatline visualization of MHD natural convection in an inclined wavy open porous cavity filled with a nanofluid with a local heater. Int J Heat Mass Transf. 2016;99:872–81.
35. Sheremet MA, Oztop H, Pop I. MHD natural convection in an inclined wavy cavity with corner heater filled with a nanofluid. J Magn Magn Mater. 2016;416:37–47.
36. Rashad A, Chamkha AJ, Ismael MA, Salah T. Magnetohydrodynamics natural convection in a triangular cavity filled with a Cu–Al_2O_3/water hybrid nanofluid with localized heating from below and internal heat generation. J Heat Transf. 2018;140(7):072502.
37. Alsabery AI, Ismael MA, Chamkha AJ, Hashim I. Effects of two-phase nanofluid model on MHD mixed convection in a lid-driven cavity in the presence of conductive inner block and corner heater. J Therm Anal Calorim. 2018. https://doi.org/10.1007/s10973-018-7377-6.
38. Ismael MA, Ghalib HS. Double diffusive natural convection in a partially layered cavity with inner solid conductive body. Sci Iran. 2018;25(5):2643–59.
39. Alsabery AI, Hashim I, Chamkha AJ, Saleh H, Chanane B. Effect of spatial side-wall temperature variation on transient natural convection of a nanofluid in a trapezoidal cavity. Int J Numer Methods Heat Fluid Flow. 2017;27(6):1365–84.
40. Alsabery AI, Tayebi T, Chamkha AJ, Hashim I. Effect of rotating solid cylinder on entropy generation and convective heat transfer in a wavy porous cavity heated from below. Int Commun Heat Mass Transf. 2018;95:197–209.
41. Alsabery A, Ismael M, Chamkha A, Hashim I. Numerical investigation of mixed convection and entropy generation in a wavy-walled cavity filled with nanofluid and involving a rotating cylinder. Entropy. 2018;20(9):664.
42. Alsabery AI, Armaghani T, Chamkha AJ, Hashim I. Conjugate heat transfer of Al_2O_3–water nanofluid in a square cavity heated by a triangular thick wall using Buongiorno's two-phase model. J Therm Anal Calorim. 2018. https://doi.org/10.1007/s10973-018-7473-7.
43. Mehryan SAM, Ghalambaz M, Izadi M. Conjugate natural convection of nanofluids inside an enclosure filled by three layers of solid, porous medium and free nanofluid using Buongiorno's and local thermal non-equilibrium models. J Therm Anal Calorim. 2018. https://doi.org/10.1007/s10973-018-7380-y.
44. Tahmasebi A, Mahdavi M, Ghalambaz M. Local thermal nonequilibrium conjugate natural convection heat transfer of nanofluids in a cavity partially filled with porous media using Buongiorno's model. J Numer Heat Transf A Appl. 2018;73(4):254–76.
45. Jena P, Brocchi E, Motta M. In-situ formation of Cu–Al_2O_3 nano-scale composites by chemical routes and studies on their microstructures. Mater Sci Eng A. 2001;313(1–2):180–6.
46. Suresh S, Venkitaraj K, Selvakumar P, Chandrasekar M. Synthesis of Al_2O_3–Cu/water hybrid nanofluids using two step method and its thermo physical properties. Colloids Surf A. 2011;388(1–3):41–8.
47. Chamkha A, Doostanidezfuli A, Izadpanahi E, Ghalambaz M. Phase-change heat transfer of single/hybrid nanoparticles-enhanced phase-change materials over a heated horizontal cylinder confined in a square cavity. Adv Powder Technol. 2017;28(2):385–97.
48. Ghalambaz M, Doostani A, Chamkha AJ, Ismael MA. Melting of nanoparticles-enhanced phase-change materials in an enclosure: effect of hybrid nanoparticles. Int J Mech Sci. 2017;134:85–97.
49. Ghalambaz M, Doostani A, Izadpanahi E, Chamkha AJ. Phase-change heat transfer in a cavity heated from below: the effect of utilizing single or hybrid nanoparticles as additives. J Taiwan Inst Chem Eng. 2017;72:104–15.
50. Suresh S, Venkitaraj K, Selvakumar P, Chandrasekar M. Effect of Al_2O_3–Cu/water hybrid nanofluid in heat transfer. Exp Therm Fluid Sci. 2012;38:54–60.
51. Ismael MA, Armaghani T, Chamkha AJ. Mixed convection and entropy generation in a lid-driven cavity filled with a hybrid nanofluid and heated by a triangular solid. Heat Transf Res. 2018;49(17):1645–65.
52. Esfe MH, Arani AAA, Rezaie M, Yan W-M, Karimipour A. Experimental determination of thermal conductivity and dynamic viscosity of Ag–MgO/water hybrid nanofluid. Int Commun Heat Mass Transf. 2015;66:189–95.
53. Moghadassi A, Ghomi E, Parvizian F. A numerical study of water based Al_2O_3 and Al_2O_3–Cu hybrid nanofluid effect on forced convective heat transfer. Int J Therm Sci. 2015;92:50–7.
54. Mehryan S, Kashkooli FM, Ghalambaz M, Chamkha AJ. Free convection of hybrid Al_2O_3–Cu water nanofluid in a differentially heated porous cavity. Adv Powder Technol. 2017;28(9):2295–305.
55. Kefayati GR. Effect of a magnetic field on natural convection in an open cavity subjugated to water/alumina nanofluid using Lattice Boltzmann method. Int Commun Heat Mass Transf. 2013;40:67–77.
56. Elshehabey HM, Hady F, Ahmed SE, Mohamed R. Numerical investigation for natural convection of a nanofluid in an inclined L-shaped cavity in the presence of an inclined magnetic field. Int Commun Heat Mass Transf. 2014;57:228–38.
57. Nasrin R, Alim M. Free convective flow of nanofluid having two nanoparticles inside a complicated cavity. Int J Heat Mass Transf. 2013;63:191–8.
58. Maxwell JC. A treatise on electricity and magnetism. Oxford: Clarendon Press; 1881.
59. Murshed S, Leong K, Yang C. Enhanced thermal conductivity of TiO_2—water based nanofluids. Int J Therm Sci. 2005;44(4):367–73.
60. Einstein A. Investigations on the theory of the Brownian movement. North Chelmsford: Courier Corporation; 1956.
61. Brinkman H. The viscosity of concentrated suspensions and solutions. J Chem Phys. 1952;20(4):571.
62. Batchelor G. The effect of Brownian motion on the bulk stress in a suspension of spherical particles. J Fluid Mech. 1977;83(1):97–117.
63. Strang G, Fix GJ. An analysis of the finite element method. Englewood Cliffs: Prentice-Hall; 1973.
64. Souli MH, Benson DJ. Arbitrary Lagrangian Eulerian and fluid-structure interaction: numerical simulation. New York: Wiley; 2013.
65. Codina R, Houzeaux G, Coppola-Owen H, Baiges J. The fixed-mesh ALE approach for the numerical approximation of flows in moving domains. J Comput Phys. 2009;228(5):1591–611.
66. Sun F. Investigations of smoothed particle hydrodynamics method for fluid-rigid body interactions. Southampton: University of Southampton; 2013.
67. Hindmarsh AC, Brown PN, Grant KE, Lee SL, Serban R, Shumaker DE, Woodward CS. SUNDIALS: Suite of nonlinear and differential/algebraic equation solvers. ACM Trans Math Softw TOMS. 2005;31(3):363–96.
68. Xu F, Patterson JC, Lei C. Heat transfer through coupled thermal boundary layers induced by a suddenly generated temperature difference. Int J Heat Mass Transf. 2009;52(21–22):4966–75.